Hv1 proton channels are required for high-level NADPH oxidase-dependent superoxide production during the phagocyte respiratory burst

I. Scott Ramsey[1], Evelyne Ruchti, J. Stefan Kaczmarek, and David E. Clapham[2]

Howard Hughes Medical Institute, Department of Neurobiology, Harvard Medical School, and Department of Cardiovascular Research, Manton Center for Orphan Disease, Children's Hospital, 320 Longwood Avenue, Boston, MA 02115

Contributed by David E. Clapham, March 16, 2009 (sent for review January 9, 2009)

Granulocytes generate a "respiratory burst" of NADPH oxidase-dependent superoxide anion ($O_2^{-\bullet}$) production that is required for efficient clearance of bacterial pathogens. Hv1 mediates a voltage-gated H^+ channel activity that is proposed to serve a charge-balancing role in granulocytic phagocytes such as neutrophils and eosinophils. Using mice in which the gene encoding Hv1 is replaced by β-Geo reporter protein sequence, we show that Hv1 expression is required for measurable voltage-gated H^+ current in unstimulated phagocytes. $O_2^{-\bullet}$ production is substantially reduced in the absence of Hv1, suggesting that Hv1 contributes a majority of the charge compensation required for optimal NADPH oxidase activity. Despite significant reduction in superoxide production, *Hv1*$^{-/-}$ mice are able to clear several types of bacterial infections.

HV1$^{-/-}$ | immunity | voltage-gated ion channel | innate immunity

The voltage-gated H^+ channel Hv1 (also termed VSOP or BTS) was identified by its homology to the voltage sensor domain of voltage-gated cation channels and a voltage-regulated phosphatase Ci-VSP (1–4). Hv1 is encoded by the *Hvcn1* gene, and both protein function and genetic sequences are well conserved from primitive chordates to mammals (1, 2). Expression of Hv1 in either mammalian cells or *Xenopus* oocytes is sufficient to reconstitute the hallmark biophysical properties of native voltage-dependent H^+ conductances (G_{vH^+}): activation by transmembrane depolarization or net intracellular acidification, exquisite H^+-selective conductance, and sensitivity to inhibition by micromolar Zn^{2+} (1, 2, 5–8). Under resting physiological conditions in most cells ($pH_i \approx pH_o$), the channel's voltage-dependent gating dictates that protons flow only outward through Hv1, suggesting that a prominent physiological role for the channel is to secrete H^+ (5).

Voltage-gated H^+ currents and Hv1 protein are prominently expressed in granulocytic phagocytes such as neutrophils and eosinophils (1, 3, 5, 9); granulocytes are characterized by their ability to mount a "respiratory burst" of high-level NADPH oxidase-dependent superoxide anion ($O_2^{-\bullet}$) production that is required for clearance of bacterial pathogens (10). NADPH oxidase would cause a rapid intracellular acidification and profound depolarization of the cell membrane in the absence of a balancing charge movement, and G_{vH^+} mediated by Hv1 is ideally suited to meet this physiological requirement (11–14). To investigate whether Hv1 is required for innate immune function, we generated an Hv1 knockout mouse (Hv1$^{-/-}$) line and assessed voltage-gated H^+ current, $O_2^{-\bullet}$ production, and bacterial clearance in Hv1$^{-/-}$ mice and their *wt*/*wt* littermates. Our results demonstrate that Hv1 is required for G_{vH^+}, a robust respiratory burst, and efficient bacterial clearance in vitro.

Results

The Bay Genomics genetrap of the *Hvcn1* locus leads to transcription of a transgenic mRNA that contains a β-Geo reporter gene sequence in place of the Hv1 protein coding sequence, such that only the 6 N-terminal residues of Hv1 are translated (Fig. S1). RRN293 ES cells bearing the *Hvcn1* genetrap allele were used to generate a transgenic mouse line that that is expected to lack Hv1 protein expression and voltage-gated proton channel activity. Triplex genomic PCR demonstrated the expected *Hvcn1* size difference for the *wt* and transgenic alleles (Fig. 1*A*), and was used in conjunction with quantitative genomic PCR for genotypic screening during breeding. Homozygous RRN293 mice lack detectable levels of Hv1 protein in spleen, bone marrow cells (BMC), and peripheral blood leukocytes (Fig. 1*B*), indicating that the genetrap strategy results in an effective Hv1 knockout (*Hv1*$^{-/-}$). Consistent with the reported expression of G_{vH^+} in alveolar epithelial cells (15, 16), we detected Hv1 protein in lung homogenates from *wt*/*wt* but not *Hv1*$^{-/-}$ mice (Fig. S1).

Hv1 protein was not detectable in hippocampal microsomes, suggesting that the lack of detectable voltage-gated H^+ current in mammalian neurons results from low Hv1 expression (17). Consistent with previous reports (18, 19) we measured G_{vH^+} in acutely isolated non-neuronal hippocampal cells (presumably microglia) but not in *Hv1*$^{-/-}$ cells. The relative paucity of microglia could account for undetectably low levels of Hv1 protein in brain, and future studies should investigate Hv1 expression and function in microglia in situ. We next measured voltage-gated whole-cell H^+ currents in leukocytes isolated from *wt*/*wt* or *Hv1*$^{-/-}$ mice as described (1). Purified resting (round and nonadherent) granulocytes exhibited G_{vH^+} at varying levels, but *Hv1*$^{-/-}$ mice lacked detectable H^+ current (Fig. 2 *B* and *D*). Consistently larger currents were measured in cells displaying the morphological characteristics (presence of pseudopodia and a uropod, spontaneous adherence and cytokinesis on glass substrate) of circulating neutrophils (Fig. 2*A*). The apparent threshold for voltage-dependent activation (V_{thr}) of H^+ currents elicited by depolarizing voltage steps was approximately +40 mV under symmetrical recording conditions (Fig. 2*C*; $pH_i = pH_o = 6.5$). As expected for authentic G_{vH^+}, V_{thr} shifted negatively ≈40 mV when a 1-log unit outward [H^+] gradient ($pH_i = 6.5$, $pH_o = 7.5$) was imposed (Fig. 2*C*) (5, 7). In no instance were we able to measure detectable voltage-activated H^+ currents in cells isolated from *Hv1*$^{-/-}$ mice (Fig. 2 *B* and *D*), indicating that Hv1 expression is required for G_{vH^+}. In combination with previous results demonstrating that Hv1 is sufficient to reconstitute G_{vH^+} (1, 2), these results suggest that Hv1 intrinsically forms the

Author contributions: I.S.R. and D.E.C. designed research; I.S.R., E.R., and J.S.K. performed research; I.S.R. contributed new reagents/analytic tools; I.S.R. analyzed data; and I.S.R. and D.E.C. wrote the paper.

The authors declare no conflict of interest.

Freely available online through the PNAS open access option.

[1]Present address: Department of Physiology and Biophysics, Virginia Commonwealth University School of Medicine, 1101 East Marshall Street, P.O. Box 980551, Richmond, VA 23298.

[2]To whom correspondence should be addressed. E-mail: dclapham@enders.tch.harvard.edu.

This article contains supporting information online at www.pnas.org/cgi/content/full/0902761106/DCSupplemental.

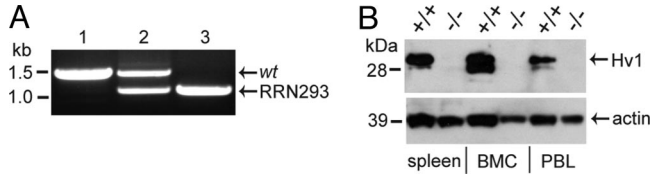

Fig. 1. Generation of *Hv1*$^{-/-}$ mice. RRN293 ES cells contain a Bay Genomics genetrap vector insertion in the *Hvcn1* gene. The transgene serves as a surrogate splice acceptor for *wt* exon 2 that produces an in-frame chimeric mRNA encoding *Hvcn1* exons 1 and 2 followed by β-Geo sequence. (*A*) Triplex genomic PCR using reverse primers specific for both *Hvcn1* and β-Geo amplifies a ≈1.5-kb band from the *wt* allele (lane 1) and a ≈1.0-kb band from the transgenic allele (lane 3); both alleles are detected in heterozygous *wt*/RRN293 mice (lane 2). (*B*) Expression of Hv1 protein (32 kDa) is readily detected in spleen (lanes 1 and 2), BMC (lanes 3 and 4), and PBL (lanes 5 and 6) isolated from *wt*/*wt* mice (+/+, lanes 1, 3, and 5) but is absent in RRN293/RRN293 mouse tissue (−/−, lanes 2, 4, and 6).

voltage-dependent proton channel that underlies G_{vH^+} in various cell types. The existence of additional genes encoding voltage-gated proton channels therefore seems unlikely. This conclusion is further supported by the observation that native G_{vH^+} and expressed Hv1 share unique biophysical properties (especially

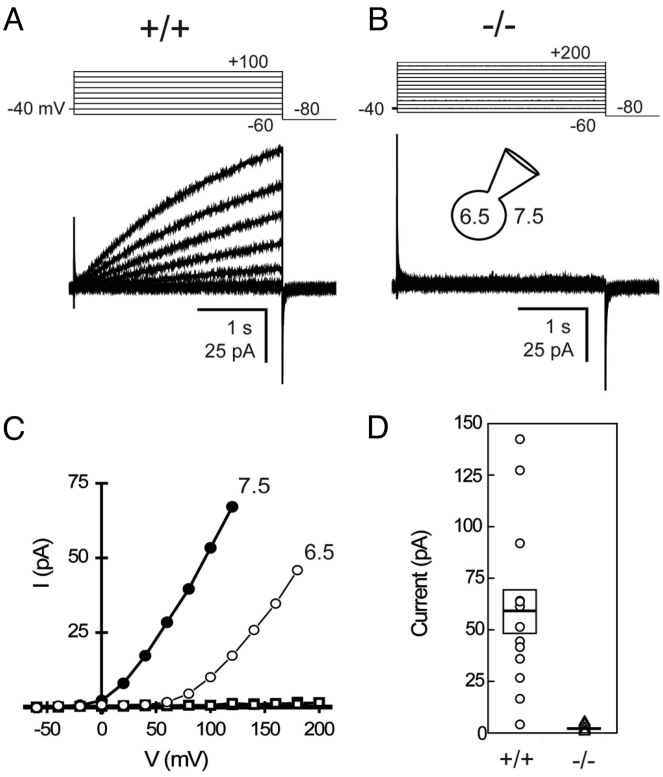

Fig. 2. RRN293/RRN293 leukocytes lack detectable voltage-gated H^+ currents. (*A* and *B*) Representative whole-cell currents (*Lower*) resulting from the indicated voltage steps (*Upper*) in neutrophils (Lympholyte M) purified from *wt*/*wt* (+/+, *Left*) or RRN293/RRN293 (−/−, *Right*) B5 mouse blood. (*Inset*) The pH of solutions (TMA6.5 pipette, TMA7.5 bath) is shown. (*C*) Representative I_{STEP} vs. voltage relations for the cells shown in *A* under symmetrical [H^+] conditions and after bath superfusion to impose a 1 pH unit outward [H^+] gradient (○, +/+ TMA6.5 bath; ●, +/+ TMA7.5 bath; □, −/− TMA6.5 bath; ■, −/−TMA7.5 bath). (*D*) Whole-cell current (I_{STEP}, +60 mV) in granulocytes (Robbins PMN) purified from *wt*/*wt* (+/+) or RRN293/RRN293 (−/−) mouse blood (Na6.5 pipette and Na7.5 bath solutions). Solid line indicates the mean current level, and box indicates SEM (+/+, 58.6 ± 10.5 pA; −/−, 2.7 ± 0.4 pA; n = 14 cells per genotype).

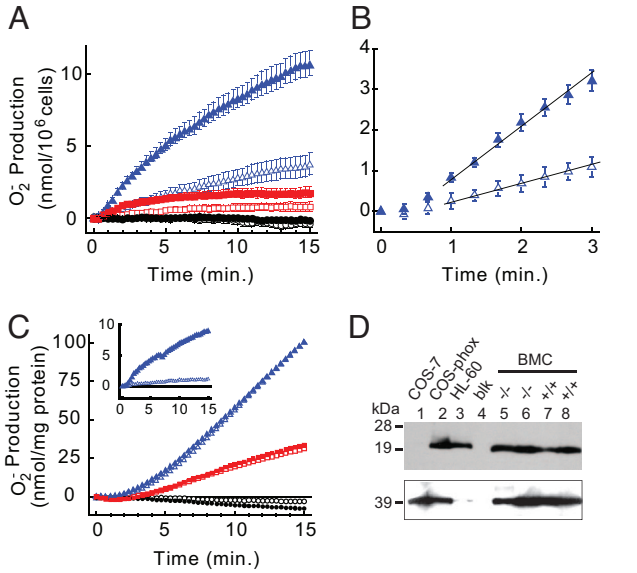

Fig. 3. Superoxide anion ($O_2^{-\bullet}$) production is decreased in *Hv1*$^{-/-}$ BMC. $O_2^{-\bullet}$ secretion was measured by using the cytochrome *c* reduction assay in intact BMC isolated from *wt*/*wt* (+/+, filled symbols) or RRN293/RRN293 (−/−, open symbols) B5 mice in the absence (black circles) or presence of 200 nM PMA (blue triangles) or 200 nM PMA + 10 μM DPI (red squares). (*A*) Time course of $O_2^{-\bullet}$ production after vehicle or PMA addition at t = 0 min in intact BMC. $O_2^{-\bullet}$ production after 10-min incubation (37 °C) in the presence of 200 nM PMA was 9.93 ± 1.24 nmol/10^6 cells (+/+) and 3.60 ± 0.18 nmol/10^6 cells (−/−); mean ± SEM, n = 4 mice per genotype). (*B*) The rates of PMA-stimulated $O_2^{-\bullet}$ production in intact BMC between 1 and 3 min after PMA addition were: +/+, 1.39 ± 0.23 nmol/min per 10^6 cells; −/−, 0.47 ± 0.04 nmol/min per 10^6 cells; mean ± SEM, n = 4 (solid lines). Data and symbols are as shown in *A*. (*C*) Time course of $O_2^{-\bullet}$ production after vehicle or AA (100 μM) addition at t = 0 min in a representative pair of *wt*/*wt* and RRN293/RRN293 littermate BMC sonicates assayed in parallel. (*Inset*) Time course of $O_2^{-\bullet}$ production after vehicle or PMA addition at t = 0 min in intact BMC before sonication. Data are expressed as nmol $O_2^{-\bullet}$/min per 10^6 cells. Open and filled symbols are as in *A*. (*D*) Western blot showing p22^{phox} expression in lysates prepared from nontransfected COS-7, COS-phox, or HL-60 cells (lanes 1–3) or BMC isolated from 2 pairs of RRN293/RRN293 (−/−, lanes 5 and 6) or *wt*/*wt* (+/+, lanes 7 and 8) mouse littermates.

the invariant coupling of V_{thr} to the pH gradient) that are conserved in a wide variety of cell types (5, 7). Cell-specific factors are likely to modulate Hv1 channel properties, particularly in cells such as neutrophils, where G_{vH^+} appears to be posttranslationally regulated by signaling cascades (20–22).

Two lines of evidence suggested that G_{vH^+} might be necessary for sustained $O_2^{-\bullet}$ production during the respiratory burst: first, outward H^+ current through Hv1 should balance the outward e^- current produced by the active NADPH oxidase, thereby limiting membrane depolarization that would otherwise inhibit NADPH oxidase activity (11–14); second, Hv1 allows for extrusion of intracellular protons that are produced by NADPH oxidase, thus limiting intracellular acidosis and maintaining optimal $O_2^{-\bullet}$ production (23–25). To test the hypothesis that Hv1 is required for high-level superoxide production, we isolated BMC from *wt* and *Hv1*$^{-/-}$ mice and measured phorbol 12-myristate 13-acetate (PMA)-stimulated $O_2^{-\bullet}$ and hydrogen peroxide (H_2O_2) production spectrophotometrically (Fig. 3 and Fig. S2). PMA (200 nM) elicited a robust time-dependent increase in $O_2^{-\bullet}$ production that was absent in vehicle-treated control cells and largely blocked by dephenylene iodonium (DPI; 10 μM), an inhibitor of NADPH oxidases (Fig. 3*A*). After an initial delay, the rate of $O_2^{-\bullet}$ production (measured 1–3 min after PMA addition at 37 °C) was attenuated ≈65% in cells from *Hv1*$^{-/-}$ mice compared with *wt*/*wt* littermates (Fig. 3*B*), and a similar decrement was observed

PHYSIOLOGY

15 min after PMA addition (Fig. 3*A*). DPI (10 μM) inhibited 79% and 73% of the PMA-stimulated $O_2^{-\bullet}$ production (at 15 min) in *wt/wt* and *Hv1*$^{-/-}$ BMC, respectively (Fig. 3*A*). Similar results were observed in peripheral blood leukocytes (PBL) purified from either Lympholyte M or discontinuous Percoll gradients, and BMC isolated from *Hv1*$^{-/-}$ mice with mixed C57BL/6J host and 129 ES cell genetic background were not significantly different from back-crossed *Hv1*$^{-/-}$ B5 mice. Finally, PMA-stimulated H_2O_2 production was also substantially decreased in *Hv1*$^{-/-}$ BMC compared with *wt/wt* controls (Fig. S2).

In contrast to intact cells, $O_2^{-\bullet}$ production was not different in a broken-cell preparation made from either *wt/wt* or *Hv1*$^{-/-}$ BMC (Fig. 3*C*). Consistent with the idea that Hv1 is required for charge compensation and H^+ efflux in intact cells but is irrelevant in membrane fragments that do not experience changes in voltage or pH gradients after NADPH oxidase activation. In addition, we observed similar levels of p22^{phox} expression in *wt/wt* and *Hv1*$^{-/-}$ BMC microsomes (Fig. 3*D*). Together, these results suggest that attenuated $O_2^{-\bullet}$ production in *Hv1*$^{-/-}$ cells is unlikely to result from a decrease in the activity or expression of NADPH oxidase complex components *per se*. Although our data do not rule out the possibility that other gene products or ion transport pathways also contribute to charge compensation during the phagocyte respiratory burst, they suggest that Hv1 is likely to play a central role in electrical and H^+ gradient homeostasis that is required for optimal NADPH oxidase activity under physiological conditions in mouse granulocytes (12, 25–32).

The role of the respiratory burst in innate immune function is illustrated by the observation that deletion or mutation in any of several protein components comprising the NADPH oxidase complex impairs bacterial clearance in mice and causes chronic granulomatous disease in humans (10). To determine whether the attenuated $O_2^{-\bullet}$ production that we observed in *Hv1*$^{-/-}$ cells would adversely affect bacterial clearance, we incubated *wt* or *Hv1*$^{-/-}$ BMC with live, serum-opsonized *Staphylococcus aureus* and assayed bacterial survival. BMC from both *wt/wt* and *Hv1*$^{-/-}$ mice cleared >90% of the added bacteria (Fig. 4*A*), suggesting that the viability and bacterial killing function of BMC isolated from both *wt/wt* and *Hv1*$^{-/-}$ mice is similar. NADPH oxidase-dependent bacterial killing was significantly attenuated in *Hv1*$^{-/-}$ compared with *wt/wt* mice (Fig. 4 *A* and *B*). Bacterial survival was similar in the presence of DPI, suggesting that NADPH oxidase-independent mechanisms of bacterial clearance were unchanged in *Hv1*$^{-/-}$ cells and that Hv1 deletion selectively affects NADPH oxidase-dependent killing. Furthermore, phagocytosis of heat-inactivated, fluorescently-labeled, serum-opsonized *S. aureus* or *E. coli* was not different in *Hv1*$^{-/-}$ and *wt/wt* cells, suggesting that the observed defect in bacterial clearance is caused by reduced $O_2^{-\bullet}$ production and not by a change in the abilty of *Hv1*$^{-/-}$ cells to phagocytose bacteria.

We next tested whether *Hv1*$^{-/-}$ mice are able to clear bacterial infections in vivo. *Hv1*$^{-/-}$ or *wt/wt* mice were inoculated i.p. with *S. aureus*, and surviving bacteria were elaborated on selective agar from peritoneal lavage fluid h 6–24 later. In mice inoculated with 1×10^8 *S. aureus* we observed a >2-log unit decrease in bacterial CFU after a 24-h incubation in vivo (Fig. 4*C*). Whereas mice that received 1×10^8 CFU of *S. aureus* did not visibly manifest sepsis, mice of either genotype that received 5×10^9 CFU were typically moribund within 6 h of inoculation. Although bacterial load in the peritoneal lavage from *Hv1*$^{-/-}$ mice suggested a trend toward decreased bacterial clearance, the data did not reach statistical significance. We also observed robust clearance of experimental pneumonia 24 h after intranasal inoculation of 1×10^8 CFU *Pseudomonas aeurginosa* or *Burkholderia cepacia* in both *wt/wt* and *Hv1*$^{-/-}$ mice. Although Hv1 deletion reduces Hv1 protein and G_{vH^+} to undetectably low levels, decreases $O_2^{-\bullet}$ production by ≈75%, and significantly attenuates bacterial killing in vitro, we were unable to see a significant effect on bacterial clearance in vivo under our experimental conditions.

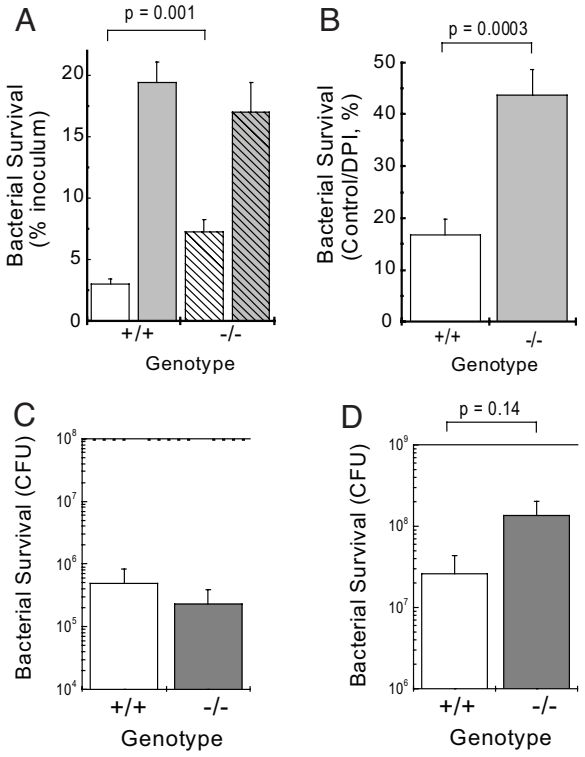

Fig. 4. Hv1 deletion decreases bacterial clearance in vitro. (*A*) Mouse BMC (5×10^5) from *wt/wt* (solid columns, $n = 8$) or RRN293/RRN293 (hatched columns, $n = 7$) mice were incubated (30 min, 37 °C) with *S. aureus* in the absence (white columns) or presence of DPI (10 μM; gray columns) before addition of gentamicin and washing. Cell pellets were lysed in 1% saponin, and surviving bacteria were serially diluted and elaborated overnight on selective agar plates. (*B*) Data shown as the fraction of surviving CFU in the absence of DPI (control) divided by the CFU surviving the presence of DPI to isolate the DPI-sensitive component of bacterial clearance (*wt/wt*, white column; RRN293/RRN293, gray column). (*C*) Bacterial survival 24 h after *i.p.* inoculation of 1×10^8 CFU *S. aureus* in *wt/wt* (white column, $n = 6$) or RRN293/RRN293 (gray column, $n = 8$) mice. (*D*) Bacterial survival 6 h after i.p. inoculation of 5×10^9 CFU *S. aureus* in *wt/wt* (white column, $n = 7$) or RRN293/RRN293 (gray column, $n = 7$) B5 mice. Data represent mean values ± SEM; indicated *P* values are from Student's unpaired *t* test.

Discussion

In summary, we demonstrate here that Hv1 is necessary for measurable G_{vH^+} in a variety of leukocytes, and previous studies showed that expression of Hv1 is sufficient to reconstitute the hallmark biophysical properties of G_{vH^+} in heterologous systems (1, 2, 5–8). Superoxide production by intact (but not broken) cells is substantially reduced in the absence of Hv1. The simplest interpretation of these results is that Hv1 serves to provide a majority of the charge compensation needed to support NADPH oxidase-mediated e^- export. Despite a significant reduction in superoxide production, *wt/wt* and *Hv1*$^{-/-}$ mice were similarly able to clear *S. aureus* infections in vivo, but differences in innate immune function may become apparent under different experimental conditions.

Similar to human patients with chronic granulomatous disease, mice bearing targeted deletions or mutations of genes encoding NADPH oxidase components manifest symptoms (e.g., dramatically decreased or undetectable $O_2^{-\bullet}$ production

and decreased bacterial clearance in vitro and in vivo) (33–36). Interestingly, mice lacking either gp91^{phox} (the product of the *Nox2* gene) or inducible nitric oxide synthase (the *Nos2* gene product) exhibited a similarly modest impairment in the innate immune response to *S. aureus* challenge. In vivo, Nox2$^{-/-}$/Nos2$^{-/-}$ (double-knockout) mice required administration of oral antibiotics for survival even in the absence of bacterial challenge, suggesting that normal innate immune function relies on at least partially redundant systems for bacterial clearance (37). Thus, superoxide- and nitric oxide-dependent systems appear to function synergistically for bacterial clearance in vivo. Reconstitution of a small fraction of the total superoxide-generating capacity of the innate immune system in gp91^{phox} (*Nox2*$^{-/-}$) knockout mice was sufficient to significantly restore bacterial clearance, suggesting the presence of enormous excess capacity for NADPH oxidase-dependent superoxide production in normal granulocytes (38–40). Because $O_2^{-\bullet}$ generation was decreased ≈75% in *Hv1*$^{-/-}$ mice, the lack of a significant in vivo impairment in bacterial clearance in these mice is perhaps not surprising. *Hv1*$^{-/-}$ mice should be useful for investigating the physiological role of Hv1 in cells and tissues outside of the innate immune system in the future.

Materials and Methods

Hv1 Knockout Mice. Mice lacking functional Hv1 protein were derived from the Bay Genomics genetrap of the *Hvcn1* locus (dbGSS7585445; gi37500117). The exogenous genetrap vector sequence, containing an in-frame splice acceptor site followed by coding sequence for a β-galactosidase/neomycin (β-Geo) fusion protein, was inserted into a large (13.6 kb) intron following exon 2, which contains the Hv1 translation initiation codon. Chimeric male mice were derived from sequence-verified RRN293 genetrap ES cells and used to establish heterozygous wt/RRN293 founders; homozygous offspring were generated from heterozygous mating pairs (Mutant Mouse Regional Resource Center, Davis, CA). *Hv1*$^{-/-}$ mice backcrossed against C57/BL6J for 5 generations are designated B5. All animal husbandry and experimental procedures were approved by and performed in accordance with guidelines of the Children's Hospital Boston Institutional Animal Care and Use Committee.

Mouse Genotyping. The genomic locus of the Bay Genomics genetrap vector (*pGTOLxf*) insertion was identified by PCR using a series of forward primers spaced at 1- to 2-kb intervals in the predicted intronic *Hvcn1* sequence, along with a β-*Geo*-specific reverse primer (β-*GeoR*: 5′-GACAGTATCGGCCTCAGGAAGATCG-3′) to amplify a product containing the *pGTOLxf* insertion site. DNA sequencing of the PCR product (Mental Retardation/Developmental Disabilities Research Center Molecular Genetics Core Facility at Children's Hospital) indicated that the *pGTOLxf* vector was inserted after nucleotide 13899 (of 17054) in predicted intron 3 (variant 1, Fig. S1*A*). Genotypes were confirmed by triplex PCR performed on genomic DNA isolated from mouse tails using 2 gene-specific primers (*Hvcn1*F: 5′-GAGATCCATCTGCCTCCGTTATGAGTG-3′; *Hvcn1*R: 5′-CATGGTCTCAGTGATGTTAGGACGTC-3′) and β-*GeoR*. The genotypes of mice used for breeding were determined by quantitative genomic PCR (Transnetyx) using primers specific to *Hvcn1* intron 3 and *pGT0Lxf*; results from the Transnetyx genotyping strategy were verified by triplex genomic PCR. Although quantitative RT-PCR confirmed that the RRN293 transgene was expressed at the expense of the *wt Hvcn1* allele (Fig. S1*C*), we were unable to detect either β-galactosidase protein [using several different anti-β-galactosidase antibodies in Western blot analysis, immunocytochemistry (ICC) or immunohistochemistry (IHC)] or activity (using X-gal staining) in spleen or BMC from *Hv1*$^{-/-}$ mice.

Quantitative RT-PCR. Total RNA (500 ng) extracted from mouse BMC (Rneasy; Qiagen) was reverse-transcribed by using an oligo(dT) primer (SuperScript 3; Invitrogen). Quantitative PCR (Real time PCR systems 7300; Applied Biosystems) was performed in a final volume of 25 μL containing 40 ng of cDNA, 300 μM primers (*Hvcn1* Ex1 Fwd: 5′-TGCAAAGGAGTGCTGCAAACTA-3′; *Hvcn1* Ex1 Rev: 5′-TCGAGTAGACGCTCCGCAAT-3′; *Hvcn1* Ex2–3 Fwd: 5′-CTCTCACTGTTGGATCTTGAGACAA-3′, *Hvcn1* Ex2–3 Rev: 5′-GGGAGCCACCTTGGTTCTG-3′; β-*Geo* Fwd: 5′-GGACGCGCGAATTGAATTA-3′, β-*Geo* Rev: 5′-CTGTTGACTGTAGCGGCTGATG-3′), and 12.5 μL of SybrGr PCR master mix (Applied Biosystems). Triplicate quantitative PCRs were performed by using BMC cDNA synthesized from *wt/wt* or RRN293/RRN293 mRNA isolated from 3 mice of each genotype. Normalized values for cycle threshold ($\Delta Ct_{wt/wt}$ and $\Delta Ct_{RRN/RRN}$) were calculated by subtracting the observed cycle threshold (C_t) for each cDNA and primer pair from the C_t observed for L8 ribosomal RNA primers (2). Relative expression of β-*Geo* (Fig. S1, primers H and I) or *Hvcn1*. Relative expression of β-Geo mRNA (Fig. S1, primers H and I) in *wt/wt* BMC and *Hvcn1* mRNA in RRN293/RRN293 BMC [Fig. S1, primers D and E (*Hvcn1* Ex 1′, 1″) or primers F and G (*Hvcn1* Ex 2–3)] was calculated by using Eqs. 1 and 2.

Eq. 1. Fractional β-Geo expression in *wt/wt* = $2^{-\Delta\Delta Ct_{\beta\text{-Geo}}}$, where $\Delta\Delta Ct_{\beta\text{-Geo}} = \Delta Ct_{wt/wt} - \Delta Ct_{RRN/RRN}$ (primers H and I) and $\Delta Ct_{wt/wt} = Ct_{Hvcn1Ex1} - Ct_{L8RNA}$ and $\Delta Ct_{wt/wt} = Ct_{\beta\text{-GeoRNA}} - Ct_{L8RNA}$.

Eq. 2. Fractional Hvcn1 expression in RRN293/RRN293 = $2^{-\Delta\Delta Ct_{Hvcn1}}$, where $\Delta\Delta Ct = \Delta Ct_{RRN/RRN} - \Delta Ct_{wt/wt}$ (primers D, E and F, G).

Isolation of Mouse Leukocytes. For measurement of $O_2^{-\bullet}$ and H_2O_2, phagocytosis, and in vitro bacterial killing assays, BMC were dispersed by trituration through a 22-G needle in ice-cold Dulbecco's Ca^{2+}- and Mg^{2+}-free PBS (D-PBS) or Ca^{2+}-free modified Tyrode's Solution (TS+EGTA: 138 NaCl, 5 KCl, 1 $MgCl_2$, 1 EGTA, 10 Hepes, pH 7.4 at 23 °C) and passed through a 40-μm mesh filter (Becton-Dickinson). Cells were centrifuged (250 × *g*, 10 min, 4 °C), resuspended to 5 × 10^6/mL in TS, and kept on ice until use. In some experiments, whole blood (collected in 2–10 mM EGTA and diluted in D-PBS) or BMC were layered onto 1.5 vol PMN isolation medium (Robbins Scientific) or 0.75 vol Lympholyte M (Cedarlane), or before centrifugal sedimentation. For Western blot analysis, the mixture of PBL contained in the fractions above the erythrocyte pellet were removed, diluted into 20 vol ice-cold D-PBS containing 1 mM EGTA, pH 7.4 (PBS/EGTA), and centrifuged for 10 min at 250 × *g*. Differentiated HL-60 and COS-phox cells (gift of M. Dinauer, Indiana University School of Medicine) were cultured as described (1, 41).

Immunoblotting. Membranes were prepared from cell pellets or tissues by homogenization (1–2 min; Polytron) in ice-cold homogenization solution, 150 mM NaCl, 10 mM Tris·HCl (pH 7.2), 1 mM EDTA containing 0.3 M sucrose and protease inhibitor mixture (Complete mini; Roche; mammalian cell protease inhibitor mixture; Sigma) and sonicated (3 × 5 s, 40% maximum power, Heat Systems–Ultrasonics W225) before centrifugation (10 min, 4,000 × *g*, 4 °C) to clear nuclei and particulate material. The supernatant was then centrifuged (30 min, 25,000 × *g*, 4 °C; Sorvall Ultrafuge) to pellet cell membranes. Membranes were solubilized by sonication (3 × 5 s, 25% maximum power) in 0.2 mL of ice-cold lysis buffer (TS+EGTA containing 1% Triton X-100 and protease inhibitors). Protein concentration was determined (Bradford, BioRad protein assay) and 30 μg per lane was loaded onto 4–12% Bis-Tris Novex Nu-PAGE gels (Invitrogen) for electrophoresis in Mops running buffer before transfer to a PVDF membrane. Western blots were incubated with rocking in PBST (D-PBS containing 0.5% Tween-20) blocking solution containing 5% nonfat dry milk (60 min, 24 °C). Blots were first incubated with an anti-actin (Chemicon) primary antibody (1:1,000, 2 h, 24 °C) followed by secondary antibody (goat anti-mouse HRP-conjugated IgG; Zymed; 1:100,000, 45 min, 24 °C). Immunoreactivity was detected by using ECL Advance (Amersham). Blots were stripped (20 min, 50 °C) in 67.5 mM Tris·HCl (pH 6.8), 100 mM β-mercaptoethanol, and 2% SDS and washed with PBST before sequential incubation with anti-Hv1 primary (4234, 2 h) (1) and secondary (goat anti-rabbit HRP-conjugated IgG; Zymed; 1:100,000, 45 min) antibodies.

Electrophysiology. Mouse PBL or PMN were resuspended in either TMA6.5 [100 mM Bis·Tris (pH 6.5), 80 mM TMA-$MeSO_3$, 2 mM $MgCl_2$, 4 mM HCl, 1 mM EGTA] or Na6.5 [100 mM Bis·Tris (pH 6.5), 80 mM NaCl, 10 mM $MgCl_2$, 1 mM EGTA]. Cells were visually selected and subjected to whole-cell voltage clamp under symmetrical conditions (pipette solution same as bath solution). We also recorded currents from either crude BMC or Percoll gradient-purified BMC neutrophils; in no case did we measure voltage-dependent H^+ current in cells isolated from RRN293/RRN293 mice.

$O_2^{-\bullet}$ and H_2O_2 Production Assay (Cuvette Format). BMC were resuspended in modified Tyrode's solution [TS: 138 NaCl, 5 KCl, 1.8 $CaCl_2$, 1 $MgCl_2$, 10 Hepes (pH 7.4) at 23 °C] on ice. Phase-dark cells were counted (after 5 min at 24 °C) with a glass hemacytometer and diluted to 5 × 10^6/mL in ice-cold TS. Cells (0.1× final volume) were added to individual cuvettes containing TS plus 100 μM cytochrome *c* (or 5 μM Amplex Ultra Red and 0.5 unit/mL horseradish peroxidase for H_2O_2 production assay) with or without DPI (10 μM) or $ZnCl_2$ (1 mM). $O_2^{-\bullet}$ and H_2O_2 production were measured at 550 nm, 37 °C, in 1.0 mL of cuvettes by using a temperature-controlled spectrophotometer fitted with an automated 6-cuvette sample changer (DU800; Beckman–Coulter). Medium containing assay reagent and indicated drugs was preincubated (37 °C) for 10

min; cells were added 5 min before addition of PMA (200 nM) or arachidonic acid (AA, 100 μM) and absorbance was measured in a final volume of 1.0 mL (cuvette assay). $O_2^{-\bullet}$ and H_2O_2 production in *wt/wt* and *Hv1*$^{-/-}$ BMC were measured in parallel assays conducted simultaneously using the automated sample changer.

H_2O_2 Production Assay (96-Well Format). BMC or HL-60 cells were centrifuged (250 $\times$ *g*, 10 min) and resuspended in TS on ice. Cells were counted and diluted to 5 $\times$ 10^6/mL in ice-cold TS. Cells (20 μL) were added to individual wells containing ice-cold TS plus indicated assay reagent with or without PMA (200 nM), DPI (10 μM), or $ZnCl_2$ (1 mM). Assay plates containing added assay reagents and indicated drugs (minus PMA) were preincubated in a warm-air incubator (37 °C) for 10 min Cells were added and incubated (37 °C) for an additional 5 min. Plates were removed and $t = 0$ assigned as immediately after PMA addition. H_2O_2 secretion was measured at room temperature by using a plate-reading spectrophotometer/fluorimeter (550 $\pm$ 8-nm filter, Victor3; Wallac) in a final volume of 0.2 mL per well. All assay wells contained 5 μM Amplex Ultra Red (Invitrogen) and 0.5 unit/mL horseradish peroxidase (Zymed). In control experiments where PMA-stimulated O_2^- (cytochrome *c* reduction) and H_2O_2 (Amplex Ultra red) were measured side by side in a heated cuvette-reading spectrophotometer (1.0-mL assay volume), we observed only a small delay in H_2O_2 generation compared with O_2^- production, suggesting that the slow time course observed in some experiments (Fig. S2) was attributable to slow heating and reheating of the reagents and plates in the 37 °C warm air incubator between time points that were measured using the nonheated spectrophotometric plate reader.

In Vitro Bacterial Killing. Aliquots of bacterial stocks (stored at −80 °C in 20% glycerol) on dry ice were scraped with a sterile needle and bacteria were spread on selective agar plates (*S. aureus*: mannitol, Molecular Toxicology; *P. aeurginosa*: cetrimide, PML Microbiologicals; *B. cepacia*: BCSA, PML Microbiologicals) and grown overnight at 37 °C. LB medium was subsequently inoculated and liquid cultures were grown with shaking at 37 °C to an $OD_{600} \approx 0.5$. The concentration of bacterial CFU was calculated ($OD_{600} = 0.5$, CFU = 5 $\times$ 10^5/μL) and verified for each bacterial preparation by serial dilution and plating onto selective agar plates. Bacteria were centrifuged (10 min, 1,000 $\times$ *g*, 4 °C) and resuspended and opsonized in mouse serum containing 0.05% Tween-20 (30 min with rotation, 24 °C). Opsonized bacteria were then diluted into TS containing 0.05% Tween-20 to 2 $\times$ 10^4 CFU/μL. BMC were resuspended in ice-cold TS (10^6 cells per 100 μL) and added to round-bottom tubes containing TS solution with or without DPI (10 μM). The assay was initiated by addition of bacteria (50 μL) and allowed to proceed for 30 min (37 °C, orbital shaking) before addition of gentamicin (50 μg/mL; Sigma) and centrifugation (10 min, 2,800 $\times$ *g*, 24 °C). Cell pellets were washed in TS + EGTA and lysed by resuspension in saponin (1% in water) and 1 freeze-thaw cycle. Lysates were serially diluted and plated onto selective LB agar for overnight culture (37 °C) for manual determination of bacterial CFU. Although DPI reproducibly inhibited killing of bacteria under these experimental conditions, a large fraction of the inoculum survived even in the presence of DPI (Fig. 4*A*), suggesting that mouse BMC may use NADPH oxidase-independent mechanisms for bacterial killing that are not prominent in purified, circulating human neutrophils and/or that incomplete cell lysis may have led to an underestimate of the DPI-dependent fraction of bacterial killing (42). Our results should therefore be interpreted as a lower limit on the effect of Hv1 deletion on bacterial killing by the NADPH oxidase system.

In Vivo Bacterial Clearance. Bacteria were grown to $OD_{600nm} \approx 0.5$, centrifuged (10 min, 1,000 $\times$ *g*, 4 °C), and resuspended in sterile 0.9% NaCl or D-PBS to a final concentration of 2 $\times$ 10^8 CFU/mL (i.p.) or 2 $\times$ 10^{10} CFU/ml (intranasal) for inoculation. Mice were allowed to recover for 18–24 h after i.p. or intranasal inoculation before peritoneal (3 $\times$ 5 mL of D-PBS, 4 °C) or lung lavage (3 $\times$ 0.8 mL of D-PBS, 4 °C), respectively. Lavage fluid was centrifuged (10, 1,000 $\times$ *g*, 4 °C) and the pellet was resuspended in D-PBS containing 0.05% Tween-20 (PBST), then serially diluted in PBST before plating on selective agar plates for culture at 37 °C for 24–48 h.

Phagocytosis Assay. BMC (1 $\times$ 10^5 cells per well) were added to a 96-well plate and incubated in 0.2 mL of TS (60 min, 37 °C) to promote adherence. The supernatant was aspirated and replaced with prewarmed TS with or without DPI (10 μM) and the assay was initiated by addition of heat-inactivated Alexa Fluor 488-labeled *E. coli* K-12 Bioparticles (Invitrogen) resuspended in TS per the manufacturer's directions. After phagocytosis (120 min, 37° C), trypan blue solution (100 μL) was added to each well to quench fluorescence of nonphagocytosed extracellular bacterial particles and quickly (1 min, 24 °C incubation) aspirated. Fluorescence of phagocytosed bacterial particles was measured on a plate-treading fluorimeter (Wallac Victor3; excitation 488 nm, lowpass filter 520 nm).

ACKNOWLEDGMENTS. This work was supported by National Institutes of Health Grant T32 HLO7572 (to I.S.R. and the Department of Pediatrics, Children's Hospital). The Mental Retardation/Developmental Disabilities Research Center Molecular Genetics Core Facility at Children's Hospital is supported by National Institutes of Health Grant P30-HD18655.

1. Ramsey IS, Moran MM, Chong JA, Clapham DE (2006) A voltage-gated proton-selective channel lacking the pore domain. *Nature* 440:1213–1216.
2. Sasaki M, Takagi M, Okamura Y (2006) A voltage sensor-domain protein is a voltage-gated proton channel. *Science* 312:589–592.
3. Suenaga T, et al. (2007) Cloning of B cell-specific membrane tetraspanning molecule BTS possessing B cell proliferation-inhibitory function. *Eur J Immunol* 37:3197–3207.
4. Murata Y, Iwasaki H, Sasaki M, Inaba K, Okamura Y (2005) Phosphoinositide phosphatase activity coupled to an intrinsic voltage sensor. *Nature* 435:1239–1243.
5. DeCoursey TE (2003) Voltage-gated proton channels and other proton transfer pathways. *Physiol Rev* 83:475–579.
6. Koch HP, et al. (2008) Multimeric nature of voltage-gated proton channels. *Proc Natl Acad Sci USA* 105:9111–9116.
7. Musset B, et al. (2008) Detailed comparison of expressed and native voltage-gated proton channel currents. *J Physiol (London)* 586:2477–2486.
8. Tombola F, Ulbrich MH, Isacoff EY (2008) The voltage-gated proton channel Hv1 has two pores, each controlled by one voltage sensor. *Neuron* 58:546–556.
9. DeCoursey TE, Cherny VV (1993) Potential, pH, and arachidonate gate hydrogen ion currents in human neutrophils. *Biophys J* 65:1590–1598.
10. Heyworth PG, Cross AR, Curnutte JT (2003) Chronic granulomatous disease. *Curr Opin Immunol* 15:578–584.
11. DeCoursey TE, Morgan D, Cherny VV (2003) The voltage dependence of NADPH oxidase reveals why phagocytes need proton channels. *Nature* 422:531–534.
12. Henderson LM, Chappell JB, Jones OT (1987) The superoxide-generating NADPH oxidase of human neutrophils is electrogenic and associated with an H+ channel. *Biochem J* 246:325–329.
13. DeCoursey TE (2008) Voltage-gated proton channels. *Cell Mol Life Sci* 65:2554–2573.
14. Rada BK, Geiszt M, Hably C, Ligeti E (2005) Consequences of the electrogenic function of the phagocytic NADPH oxidase. *Philos Trans R Soc London Ser B* 360:2293–2300.
15. DeCoursey TE (1991) Hydrogen ion currents in rat alveolar epithelial cells. *Biophys J* 60:1243–1253.
16. Murphy R, Cherny VV, Morgan D, DeCoursey TE (2005) Voltage-gated proton channels help regulate pHi in rat alveolar epithelium. *Am J Physiol* 288:L398–L408.
17. Cheng YM, Kelly T, Church J (2008) Potential contribution of a voltage-activated proton conductance to acid extrusion from rat hippocampal neurons. *Neuroscience* 151:1084–1098.
18. Eder C, DeCoursey TE (2001) Voltage-gated proton channels in microglia. *Prog Neurobiol* 64:277–305.
19. De Simoni A, Allen NJ, Attwell D (2008) Charge compensation for NADPH oxidase activity in microglia in rat brain slices does not involve a proton current. *Eur J Neurosci* 28:1146–1156.
20. Morgan D, DeCoursey TE (2003) Diversity of voltage gated proton channels. *Front Biosci* 8:1266–1279.
21. Musset B, Cherny VV, Morgan D, DeCoursey TE (2009) The intimate and mysterious relationship between proton channels and NADPH oxidase. *FEBS Lett* 583:7–12.
22. Morgan D, et al. (2007) Sustained activation of proton channels and NADPH oxidase in human eosinophils and murine granulocytes requires PKC but not cPLA2 α activity. *J Physiol (London)* 579:327–344.
23. DeCoursey TE, Cherny VV, Zhou W, Thomas LL (2000) Simultaneous activation of NADPH oxidase-related proton and electron currents in human neutrophils. *Proc Natl Acad Sci USA* 97:6885–6889.
24. Henderson LM, Chappell JB, Jones OT (1988) Superoxide generation by the electrogenic NADPH oxidase of human neutrophils is limited by the movement of a compensating charge. *Biochem J* 255:285–290.
25. Rada BK, Geiszt M, Kaldi K, Timar C, Ligeti E (2004) Dual role of phagocytic NADPH oxidase in bacterial killing. *Blood* 104:2947–2953.
26. Essin K, et al. (2009) BK channels in innate immune functions of neutrophils and macrophages. *Blood* 113:1326–1331.
27. Femling JK, et al. (2006) The antibacterial activity of human neutrophils and eosinophils requires proton channels but not BK channels. *J Gen Physiol* 127:659–672.
28. DeCoursey TE, Morgan D, Cherny VV (2002) The gp91phox component of NADPH oxidase is not a voltage-gated proton channel. *J Gen Physiol* 120:773–779.
29. Petheo GL, Demaurex N (2005) Voltage- and NADPH dependence of electron currents generated by the phagocytic NADPH oxidase. *Biochem J* 388:485–491.
30. Maturana A, Krause KH, Demaurex N (2002) NOX family NADPH oxidases: Do they have built-in proton channels? *J Gen Physiol* 120:781–786.

31. Banfi B, et al. (2000) A mammalian H^+ channel generated through alternative splicing of the NADPH oxidase homolog NOH-1. *Science* 287:138–142.
32. Ahluwalia J, et al. (2004) The large-conductance Ca^{2+}-activated K^+ channel is essential for innate immunity. *Nature* 427:853–858.
33. Jackson SH, Gallin JI, Holland SM (1995) The p47phox mouse knockoutmodel of chronic granulomatous disease. *J Exp Med* 182:751–758.
34. Pollock JD, et al. (1995) Mouse model of X-linked chronic granulomatous disease, an inherited defect in phagocyte superoxide production. *Nat Genet* 9:202–209.
35. Babior BM (2004) NADPH oxidase. *Curr Opin Immunol* 16:42–47.
36. Dinauer MC (2007) Disorders of neutrophil function: An overview. *Methods Mol Biol* 412:489–504.
37. Shiloh MU, et al. (1999) Phenotype of mice and macrophages deficient in both phagocyte oxidase and inducible nitric oxide synthase. *Immunity* 10:29–38.
38. Becker S, et al. (1998) Correction of respiratory burst activity in X-linked chronic granulomatous cells to therapeutically relevant levels after gene transfer into bone marrow $CD34^+$ cells. *Hum Gene Ther* 9:1561–1570.
39. Dinauer MC, Li LL, Bjorgvinsdottir H, Ding C, Pech N (1999) Long-term correction of phagocyte NADPH oxidase activity by retroviral-mediated gene transfer in murine X-linked chronic granulomatous disease. *Blood* 94:914–922.
40. Barese CN, Goebel WS, Dinauer MC (2004) Gene therapy for chronic granulomatous disease. *Exp Opin Biol Ther* 4:1423–1434.
41. Price MO, et al. (2002) Creation of a genetic system for analysis of the phagocyte respiratory burst: High-level reconstitution of the NADPH oxidase in a nonhematopoietic system. *Blood* 99:2653–2661.
42. Decleva E, Menegazzi R, Busetto S, Patriarca P, Dri P (2006) Common methodology is inadequate for studies on the microbicidal activity of neutrophils. *J Leukocyte Biol* 79:87–94.